

David Taylor Research Center

Bethesda, MD 20084-5000

AD-A237 032



DTRC/SHD-1340-01 March 1991
Ship Hydromechanics Department

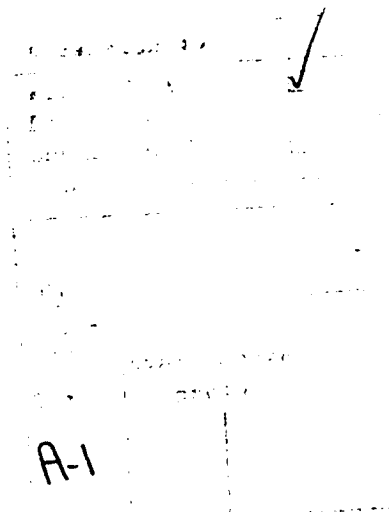


THE EFFECT OF LOCALIZED AIR EMISSION ON THE DRAG OF A SLENDER SURFACE CRAFT

by

Mark T. Coughran

David W. Coder



A-1

Original contains color plates; All DTIC reproductions will be in black and white

Approved for public release;
Distribution unlimited

DTRC/SHD-1340-01 THE EFFECT OF LOCALIZED AIR EMISSION ON THE DRAG OF A SLENDER SURFACE CRAFT



91-02353



91 02353

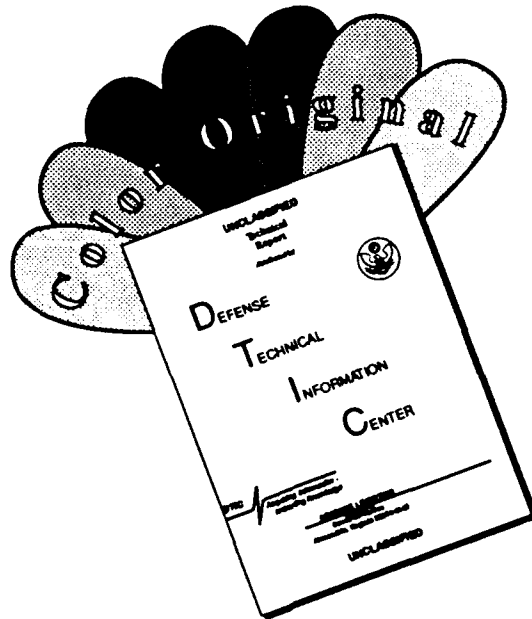
MAJOR DTRC TECHNICAL COMPONENTS

- CODE 011 DIRECTOR OF TECHNOLOGY, PLANS AND ASSESSMENT
 - 12 SHIP SYSTEMS INTEGRATION DEPARTMENT
 - 14 SHIP ELECTROMAGNETIC SIGNATURES DEPARTMENT
 - 15 SHIP HYDROMECHANICS DEPARTMENT
 - 16 AVIATION DEPARTMENT
 - 17 SHIP STRUCTURES AND PROTECTION DEPARTMENT
 - 18 COMPUTATION, MATHEMATICS & LOGISTICS DEPARTMENT
 - 19 SHIP ACOUSTICS DEPARTMENT
 - 27 PROPULSION AND AUXILIARY SYSTEMS DEPARTMENT
 - 28 SHIP MATERIALS ENGINEERING DEPARTMENT

DTRC ISSUES THREE TYPES OF REPORTS:

1. **DTRC reports, a formal series**, contain information of permanent technical value. They carry a consecutive numerical identification regardless of their classification or the originating department.
2. **Departmental reports, a semiformal series**, contain information of a preliminary, temporary, or proprietary nature or of limited interest or significance. They carry a departmental alphanumeric identification.
3. **Technical memoranda, an informal series**, contain technical documentation of limited use and interest. They are primarily working papers intended for internal use. They carry an identifying number which indicates their type and the numerical code of the originating department. Any distribution outside DTRC must be approved by the head of the originating department on a case-by-case basis.

DISCLAIMER NOTICE



THIS DOCUMENT IS BEST QUALITY AVAILABLE. THE COPY FURNISHED TO DTIC CONTAINED A SIGNIFICANT NUMBER OF COLOR PAGES WHICH DO NOT REPRODUCE LEGIBLY ON BLACK AND WHITE MICROFICHE.

UNCLASSIFIED

SECURITY CLASSIFICATION OF THIS PAGE

REPORT DOCUMENTATION PAGE

1a. REPORT SECURITY CLASSIFICATION Unclassified		1b. RESTRICTIVE MARKINGS	
2a. SECURITY CLASSIFICATION		3. DISTRIBUTION / AVAILABILITY OF REPORT Approved for public release; distribution unlimited	
2b. DECLASSIFICATION / DOWNGRADING SCHEDULE			
4. PERFORMING ORGANIZATION REPORT NUMBER(S) DTRC/SHD-1340-01		5. MONITORING ORGANIZATION REPORT NUMBER(S)	
6a. NAME OF PERFORMING ORGANIZATION David Taylor Research Center	6b. OFFICE SYMBOL <i>(If applicable)</i> Code 1543	7a. NAME OF MONITORING	
6c. ADDRESS <i>(City, State, and Zip Code)</i> Bethesda, MD 20084-5000		7b. ADDRESS <i>(City, State, and Zip Code)</i>	
8a. NAME OF FUNDING / SPONSORING ORGANIZATION Office of Naval Technology	8b. OFFICE SYMBOL <i>(If applicable)</i> ONT	9. PROCUREMENT INSTRUMENT IDENTIFICATION	
8c. ADDRESS <i>(City, State, and Zip Code)</i> 800 North Quincy St. Arlington, VA 22217-5000		10. SOURCE OF FUNDING PROGRAM ELEMENT NO. 602936	10. SOURCE OF FUNDING PROJECT NO. TASK NO. ZF66412001 WORK UNIT ACCESSION NO. DN509012
11. TITLE <i>(Include Security Classification)</i> The Effect Of Localized Air Emission On the Drag Of A Slender Surface Craft			
12. PERSONAL AUTHOR(S) Mark T. Coughran and David W. Coder			
13a. TYPE OF REPORT Departmental	13b. TIME COVERED FROM 9/88 TO 1/89	14. DATE OF REPORT <i>(Year, Month, Day)</i> 1991, March	15. PAGE COUNT 42 + vi
16. SUPPLEMENTARY NOTATION			
17. COSATI CODES FIELD GROUP SUB-GROUP		18. SUBJECT TERMS <i>(Continue on reverse if necessary and identify by block number)</i> Microbubbles Drag Reduction	
19. ABSTRACT <i>(Continue on reverse if necessary and identify by block number)</i> In an attempt to reduce skin friction drag, air bubbles were emitted from a porous girthwise section near midships on a 28 ft-(8.5 m-) long rowing shell at speeds up to 20 ft/s (6.1 m/s). Air flow rates were scaled up from previous studies which yielded large skin friction reductions on small, submerged geometries. Increases in total drag occurred in the present experiment at most conditions. The smallest-percentage drag increases occurred at the highest towing speed. Several possible reasons for the difference from the previous work are discussed.			
20. DISTRIBUTION / AVAILABILITY OF ABSTRACT <input checked="" type="checkbox"/> UNCLASSIFIED/UNLIMITED <input type="checkbox"/> SAME AS RPT <input type="checkbox"/> DTIC USERS		21. ABSTRACT SECURITY CLASSIFICATION Unclassified	
22a. NAME OF RESPONSIBLE INDIVIDUAL Mark T. Coughran		22b. TELEPHONE <i>(Include Area Code)</i> 301-227-1356	22c. OFFICE SYMBOL Code 1543

CONTENTS

ABBREVIATIONS AND SYMBOLS	v
ABSTRACT	1
ADMINISTRATIVE INFORMATION	1
INTRODUCTION	1
BACKGROUND	1
EXPERIMENTS AT ARL/PSU	3
APPLICATION OF ARL/PSU RESULTS	6
EXPERIMENTAL PROGRAM	9
MODEL	9
EXPERIMENTAL FLOW FACILITY	11
AIR JACKET	11
AIR SUPPLY SYSTEM	14
PROCEDURES	15
DRAG MEASUREMENT UNCERTAINTY	16
RESULTS	17
TOTAL DRAG MEASUREMENTS	17
VISUAL EVIDENCE	19
DRAG CHANGE DUE TO AIR EMISSION	20
DISCUSSION	25
SPEED DEPENDENCE	25
COMPARISON WITH ARL/PSU RESULTS	25
POSSIBLE MECHANISMS CAUSING DRAG INCREASES	27
CONCLUSIONS	28
RECOMMENDATIONS	29
ACKNOWLEDGMENTS	30
APPENDIX A. BOUNDARY LAYER FLOW RATE ESTIMATES	31
APPENDIX B. AIR JACKET PERFORMANCE	35
APPENDIX C. DATA	39
REFERENCES	41

FIGURES

1. Plate-on-top data of Madavan et al. (1984a)	5
2. Axisymmetric body data of Deutsch & Castano (1986)	5
3. ARL/PSU flat plate data normalized by Eq. 2	8
4. ARL/PSU axisymmetric body data normalized by Eq. 2	8
5. Model shape at $x = 14.5$ ft (4.42 m) from the forward perpendicular	10
6. Air jacket fastened to shell prior to fairing installation	13
7. Cross section "A-A" of air jacket	13
8. Shift in zero-air-flow-rate results relative to envelope of results.	18
9. Results at all towing speeds and air flow rates	18
10. Zero air flow rate runs illustrating (a) wax fairing and (b) ventilation	21
11. Low speed and high flow rate condition ($U = 4$ ft/s, $Q_a = 35$ cfm; $Q_a/Q_w = 0.52$)	21
12. High speed runs	22
13. Estimated effect on drag aft of air jacket	24
14. Rough comparison with ARL/PSU data	24
B1. Pressure drop of 10 μ m porous metal configurations	36
B2. Details of air jacket air flow resistance	36

TABLES

A1. Q_w estimates at $x_{LE} = 0.089$ m	32
A2. Q_w estimates at $x_{TW} = 0.1005$ m	33
A3. Q_w estimates at $x_{FP} = 14.5$ ft	34

ABBREVIATIONS AND SYMBOLS

A,B,C	regression coefficients
A_m	wetted area of model
ARL/PSU	Applied Research Laboratory at Pennsylvania State University
b	spanwise width of porous section
cfm	unit of flow rate, ft ³ /min
C_F	skin friction component of body drag
$C_{F,0}$	skin friction for unmodified boundary layer; $Q_a = 0$
C_T	total drag coefficient
$C_{T,0}$	total drag coefficient with $Q_a = 0$
FP	forward perpendicular
F_n	Froude number
L	wetted length
q	air flux through porous metal, Q_a/S (cfm/ft ²)
Q_a	air flow rate
Q_w	flow rate of water through the boundary layer
Q'	normalized air flow rate
R_n	length Reynolds number
R_T	total drag force
S	area of porous section
U_∞	freestream velocity
x	axial distance

ABBREVIATIONS AND SYMBOLS (continued)

Greek letters

δ	boundary layer 99 percent velocity thickness
δ^*	boundary layer displacement thickness
ρ	density
θ	boundary layer momentum thickness
ν	kinematic viscosity

ABSTRACT

In an attempt to reduce skin friction drag, air bubbles were emitted from a porous girthwise section near midships on a 28 ft-(8.5 m-) long rowing shell at speeds up to 20 ft/s (6.1 m/s). Air emission rates were scaled up from previous studies which yielded large skin friction reductions on small, submerged geometries. Increases in total drag occurred in the present experiment at most conditions. The smallest-percentage drag increases occurred at the highest towing speed. Several possible reasons for the difference from the previous work are discussed.

ADMINISTRATIVE INFORMATION

The work described in this report was performed for the David Taylor Research Center (DTRC) Independent Exploratory Development program, under Program Element 602936N, Task No. ZF66412001, and the DTRC FY-89 work unit number 1-1543-133. The experiment was a joint project with the United States Naval Academy (USNA) through the Trident Scholar Research Program.

INTRODUCTION

BACKGROUND

Drag reduction techniques have long been of interest for marine vehicles and weapons. The benefits of a successful drag reduction method include lower power requirements for a fixed speed, or a greater speed or cruise range for fixed power. Various methods have been explored for reducing the turbulent skin friction resistance. Each method has advantages and disadvantages, as summarized in the following paragraphs.

The dramatic drag-reducing effects of dilute polymers are well known for internal flows (Hoyt, 1972). For external flows, an early experiment by Canham et al. (1971)

indicated that polymers can reduce the drag of a ship. Attempts to release polymers into the boundary layer using ablative coatings (Thew et al., 1977) have seen little success.

The riblet technique has been thoroughly explored since skin friction reduction was first reported by Walsh & Weinstein (1979). However, the maximum friction reduction of approximately 8 percent for riblets is an order of magnitude smaller than the maximum reductions achieved by injection of polymers or air.

The idea of creating a layer of air next to a vessel is very old. Bogdevich et al. (1977) discuss suggestions made over 100 years ago. The difficulty of maintaining a stable air layer prevented the idea from being technically feasible. More recently, means were developed to create small bubbles of gas locally. McCormick & Bhattacharyya (1973) used electrolysis on fine wires wrapped around a submerged axisymmetric body 3 ft (0.9 m) long. A total drag reduction of approximately 10 percent was reported at the highest test speed of 6.5 ft/s (2.0 m/s), corresponding to a Reynolds number (R_n) of 1.9×10^6 . Drag reductions of 30 to 40 percent were reported at lower speeds. Further tests of the electrolysis method, using a surface ship model 18.2 ft (5.54 m) long, were reported by Thornton (1974) in collaboration with McCormick. Only 2.3 percent drag reduction was measured at the highest test speed of 5 ft/s (1.5 m/s, $R_n = 9 \times 10^6$).

Both of the above experiments used a limited current supply in fresh water. McCormick & Bhattacharyya (1973) suggested that drag reduction by electrolysis should be more practical in sea water because of its lower electrical resistance. However, recent experiments by Brown (1990) in salt water using much larger electrical current were not encouraging. In the latter experiments, a plate 6 ft (1.8 m) long was towed vertically with two adjoining plates acting as anodes. Towing speeds ranged from 2.5 ft/s (0.76 m/s) to 40 ft/s (12 m/s) corresponding to a R_n range of 1.2×10^6 to 22×10^6 . Drag increases occurred at

the lowest speeds and no measurable drag changes occurred above approximately 5 ft/s (1.5 m/s).

Another method of reducing skin friction, chosen for the present study, is to produce bubbles by forcing air through porous media. Several Soviet studies using this method have been summarized in the more recent papers by Madavan et al. (1984a) and others from the Applied Research Laboratory at Pennsylvania State University (ARL/PSU). The ARL/PSU experiments, performed on simple geometries submerged in water tunnels, will be discussed in the next section. In the present work, emphasis was placed on the surface craft application, for which there is an unlimited supply of air. The model chosen for the present experiment had a relatively high fraction of viscous drag, approximately 85 percent at the highest test speed. For common ship applications, the skin friction makes up approximately half the total drag. Operational issues such as corrosion and biofouling of the porous media are beyond the scope of the present work.

EXPERIMENTS AT ARL/PSU

Madavan et al. (1984a) performed one experiment in a zero pressure gradient turbulent boundary layer on the wall of a water tunnel. Drag was measured on a floating element balance 4.0 in. (10.2 cm) wide and 10.0 in. (25.4 cm) long. Microbubbles were generated on an upstream porous section 4.0 in. (10.2 cm) wide and 7.0 in. (17.8 cm) long. The measuring plate could be mounted on the top, bottom, or vertical side of the tunnel to study buoyancy effects. The porous stainless steel section used had a nominal filter rating of 0.5 μm , corresponding to a nominal pore size of 0.0002 in. (5.0 μm). A second experiment, by Deutsch & Castano (1986), used an axisymmetric body with a diameter of 3.5 in. (8.9 cm).

The 10.7 in.-(237 mm-) long parallel section of the body floated free of the nose and mounting sting on a force measuring gauge. A nominal pore size of 0.0002 in. (5 μm) was used in an axisymmetric injection section 0.25 in. (6.35 mm) long in the streamwise direction.

The major results of these two studies were C_F reduction with air injection of up to 85 percent with the plate-on-top configuration and up to 55 percent with the axisymmetric body. Figures 1 and 2 show these results, respectively, where the abscissa is the flow rate of air Q_a . $C_{F,0}$ represents the total skin friction coefficient for the standard or unmodified boundary layer. The plate-on-top results in Figure 1 indicate drag reduction improving as the speed is decreased. The speed trends are less clear for the axisymmetric body. At the lowest speed of 15 ft/s (4.6 m/s), only about 20 percent maximum drag reduction was achieved. Deutsch & Castano explained this result in terms of a threshold speed (≈ 25 ft/s for this body) below which buoyancy would tend to lift the bubbles away from the body. Madavan et al. (1984a) observed an unsteady "roll-up" phenomenon on the vertical plate at speeds below 8 ft/s (2.5 m/s). However, they presented evidence that the strongly modified boundary layer remained attached to the plate for all other conditions.

Further work developed the following additional information. Madavan et al. (1984b) demonstrated that pore size is not a significant factor. Measurements with hot-film probes by Madavan et al. (1985) verified large local skin friction reductions. Extrapolation of the results indicated that drag reduction persisted to approximately 70 boundary layer thicknesses downstream from the emission point. Photographic and optical studies by Pal et al. (1988) illustrated the gross appearance of the microbubbles and documented the bubble sizes.

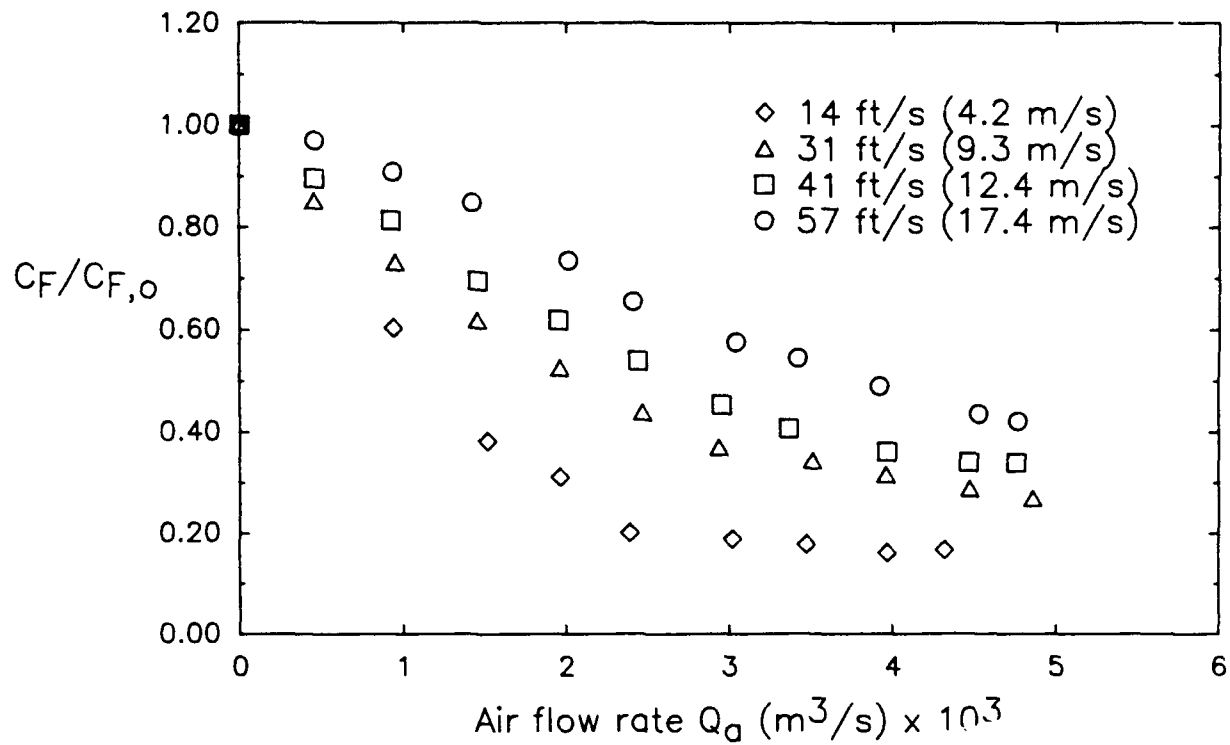


Figure 1. Plate-on-top data of Madavan et al. (1984a).

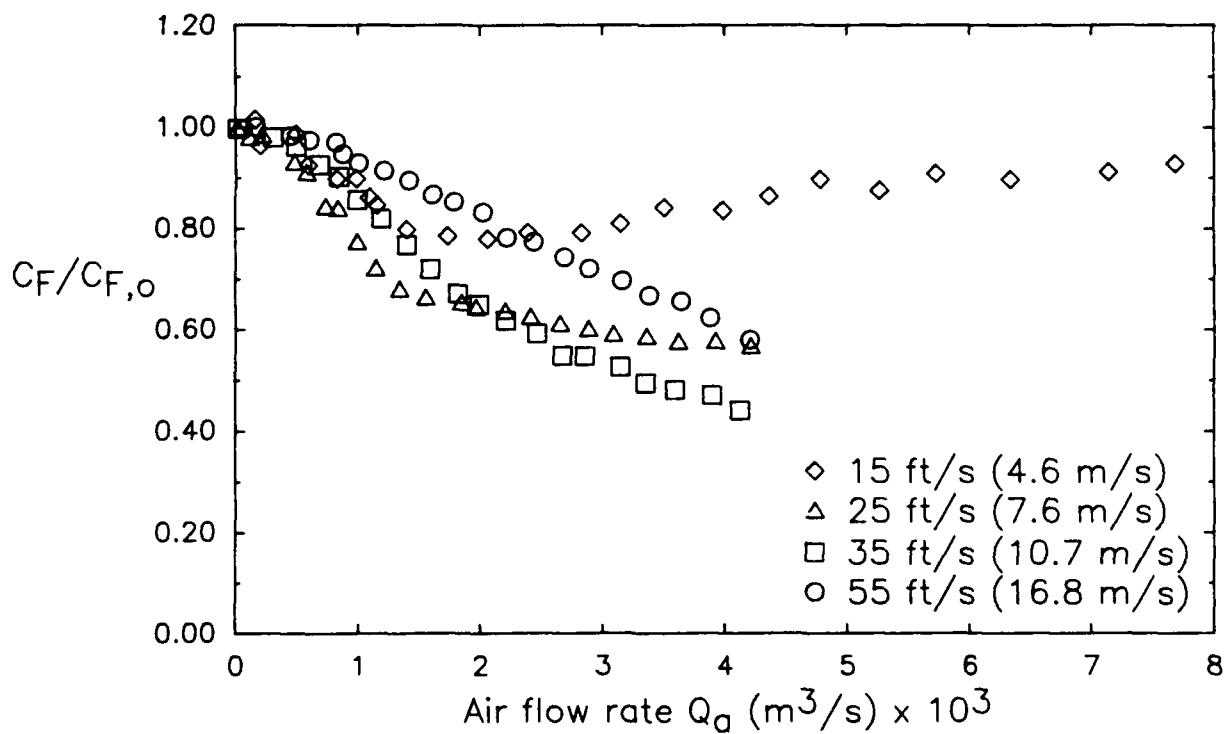


Figure 2. Axisymmetric body data of Deutsch & Castano (1986).

APPLICATION OF ARL/PSU RESULTS

The ARL/PSU air flow rates were scaled up for the present experiment, which involved higher Reynolds numbers and thicker boundary layers than used at ARL/PSU. This approach was taken because formal understanding of the mechanism by which microbubbles cause drag reduction is lacking. Although the ARL/PSU researchers and others have speculated on the mechanism, it has not yet been revealed by experiments (the same is true for polymer drag reduction, a method which has seen many successful industrial applications despite this lack of understanding).

Madavan et al. (1984a) showed that the plate-on-top results collapsed for all speeds when Q_a was normalized with freestream velocity U_∞ and porous area S :

$$Q' = \frac{Q_a}{SU_\infty} \quad (1)$$

However, the porous area does not appear to be a natural scaling parameter, since Madavan (1984) showed that varying the length of the porous section had only minor influence on the results, and Deutsch & Castano (1986) used a porous area an order of magnitude smaller.

Normalization with local boundary layer properties would be more advantageous for scaling the results to higher Reynolds numbers. As Madavan (1984) pointed out, an abscissa normalized by the volumetric flow rate of water through the boundary layer, Q_w , would be expected to provide a good collapse. Hence

$$Q' = \frac{Q_a}{Q_w} \quad (2)$$

where

$$Q_w = U_\infty(\delta - \delta^*)b \quad (3)$$

and b is the spanwise width of the porous section. Since the boundary layer thickness δ and displacement thickness δ^* are only weak functions of U_∞ at high Reynolds numbers, Eq. 2 should collapse the results in the same manner as Eq. 1. The scaling method given by Eq. 2 implies that Q_a must equal a certain proportion of the undisturbed Q_w at the emission point.

This scaling method was partially successful for the three configurations most relevant to the present experiment. Estimates of the boundary layer properties at the midpoints of the ARL/PSU porous sections were made as described in Appendix A. The normalized data are shown in Figure 3 for the flat plate (plate-on-top as in Figure 1 and plate-vertical). The scaling method removes the speed dependence for these configurations, which kept the bubbles in the boundary layer with either buoyancy (plate-on-top) or high speed (plate vertical for the two speeds reported by ARL/PSU). Maximum skin friction reductions of 80 percent and 55 percent, respectively, occurred for the two flat plate configurations. Similarly, the axisymmetric body results shown in Figure 4 are successfully scaled at high speeds. These results collapse at 25 ft/s and above, up to $Q_a/Q_w \approx 0.25$. The data at 35 ft/s and 55 ft/s are effectively identical, although with a fixed air supply higher values of Q_a/Q_w were achieved at the lower speed.

Extending these earlier results, the present experiment tested the hypothesis that large drag reductions would be possible on a much longer body if similar normalized air flow rates were used. Considering the results for different geometries shown in Figures 3 and 4, 20 to 60 percent C_F reductions were expected on a body of arbitrary shape if $Q_a/Q_w \approx 0.4$ could be obtained. The hypothesis was expected to be valid only if high bubble concentrations were maintained near the hull and the bubble size did not change significantly along the hull.

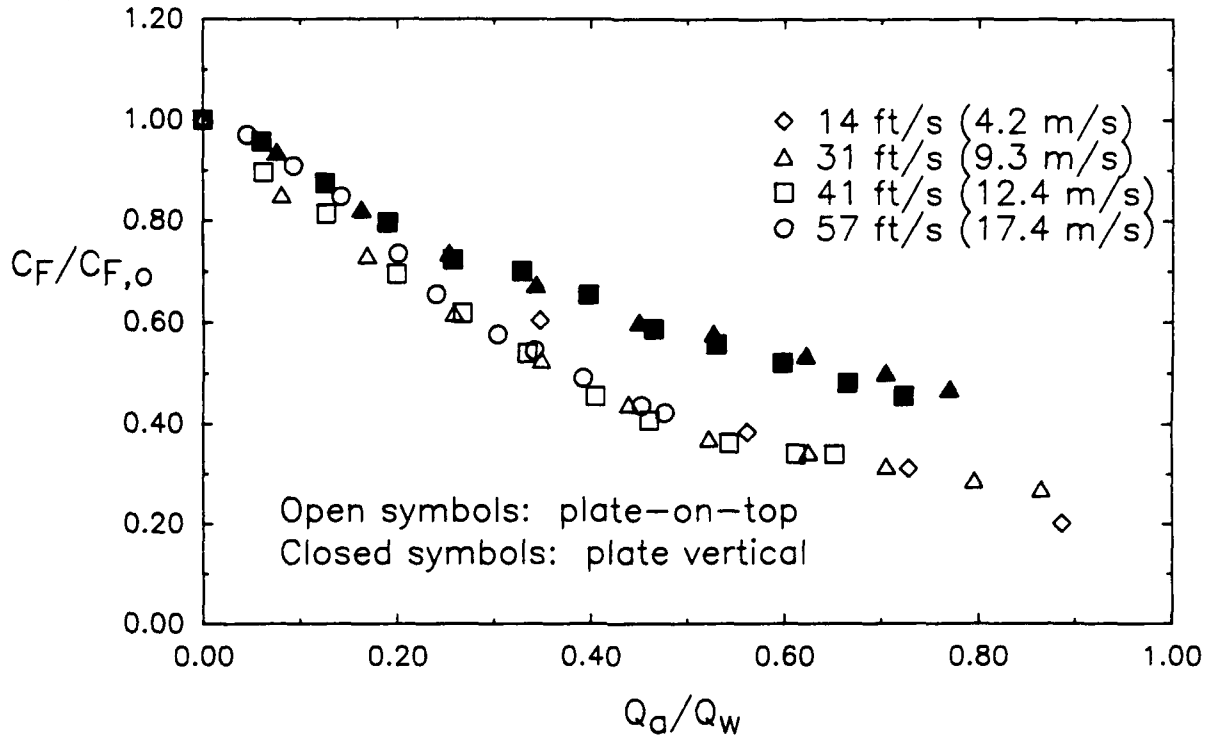


Figure 3. ARL/PSU flat plate data normalized by Eq. 2.

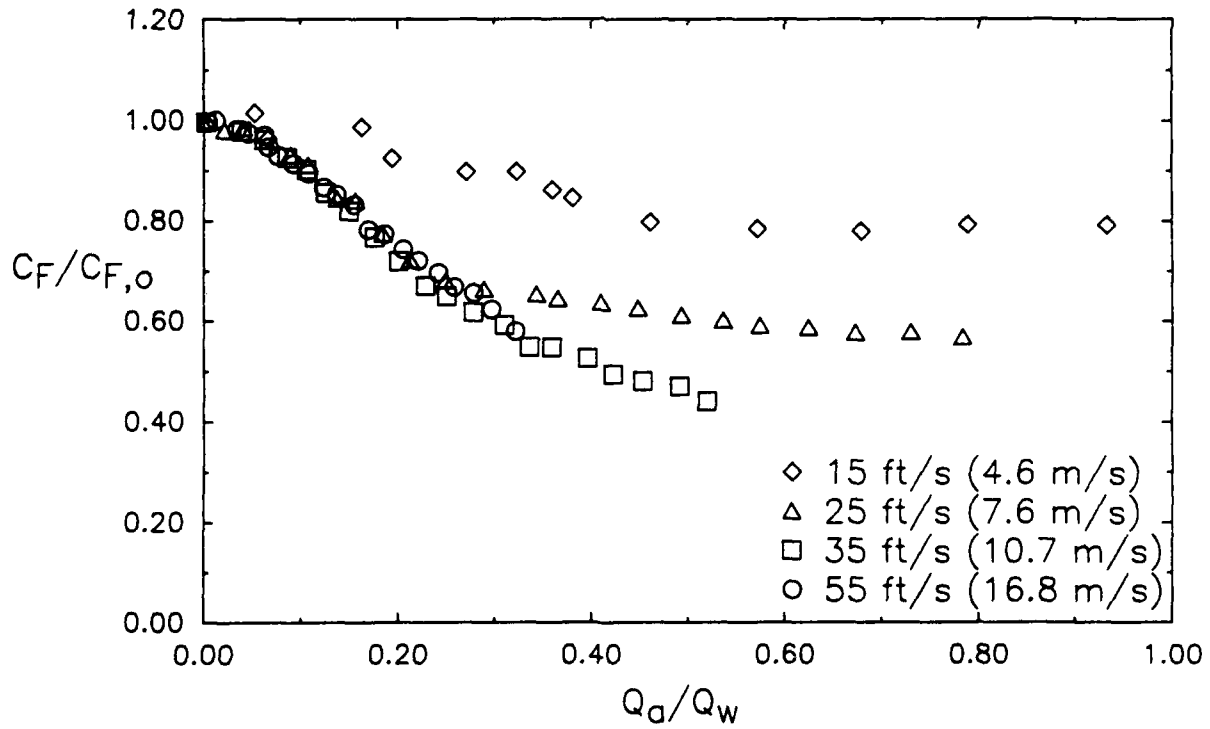


Figure 4. ARL/PSU axisymmetric body data normalized by Eq. 2.

EXPERIMENTAL PROGRAM

MODEL

The body chosen for testing was a rowing shell, nominally 28 ft (8.5 m) long, with a length between perpendiculars of 25.46 ft (7.76 m) and a midships beam of approximately 1 ft (0.3 m). The cross-sectional shape of the model near midships is shown in Figure 5. Measurements of this model by Walker (1989) in still water gave a wetted area of 26.22 ft² (2.44 m²) for a displacement of 240 lbf. A 1/8 in.(0.32 cm)-wide, 5/8 in.(1.6 cm)-high ridge around the outside of the hull on the hull center plane served as a "steering skeg". Further hull particulars are given by Coder et al. (1989) and Walker (1989). A 1/8 in.(0.32 cm)-diameter trip wire was attached around the girth of the submerged hull at 3 ft (0.9 m) from the forward perpendicular (FP). This trip wire size was chosen by Coder et al. to guarantee transition at the low speeds of particular interest in their experiments.

The leading edge of the air jacket was located at 14.5 ft (4.42 m) from the FP, slightly aft of amidships. At this location the stiffened seat area of the shell was available for clamping and the air jacket was clear of the force dynamometer and other instrumentation. This location of air injection resulted in a boundary layer thickness (δ) one order of magnitude larger than in the ARL/PSU experiments. However, the x/δ range downstream of the air injection was similar to the ARL/PSU experiments. Shell characterization measurements given by Walker (1989) show that 40 percent of the wetted area of the shell was downstream of the leading edge of the air jacket. Therefore any significant alteration of the viscous drag by air bubble injection should have been measurable. The model shape, although considerably different from the geometries used in the ARL/PSU work, resembled the lower part of an axisymmetric body combined with the plate-on-top case near midships and blending to the plate-vertical case near the stern.

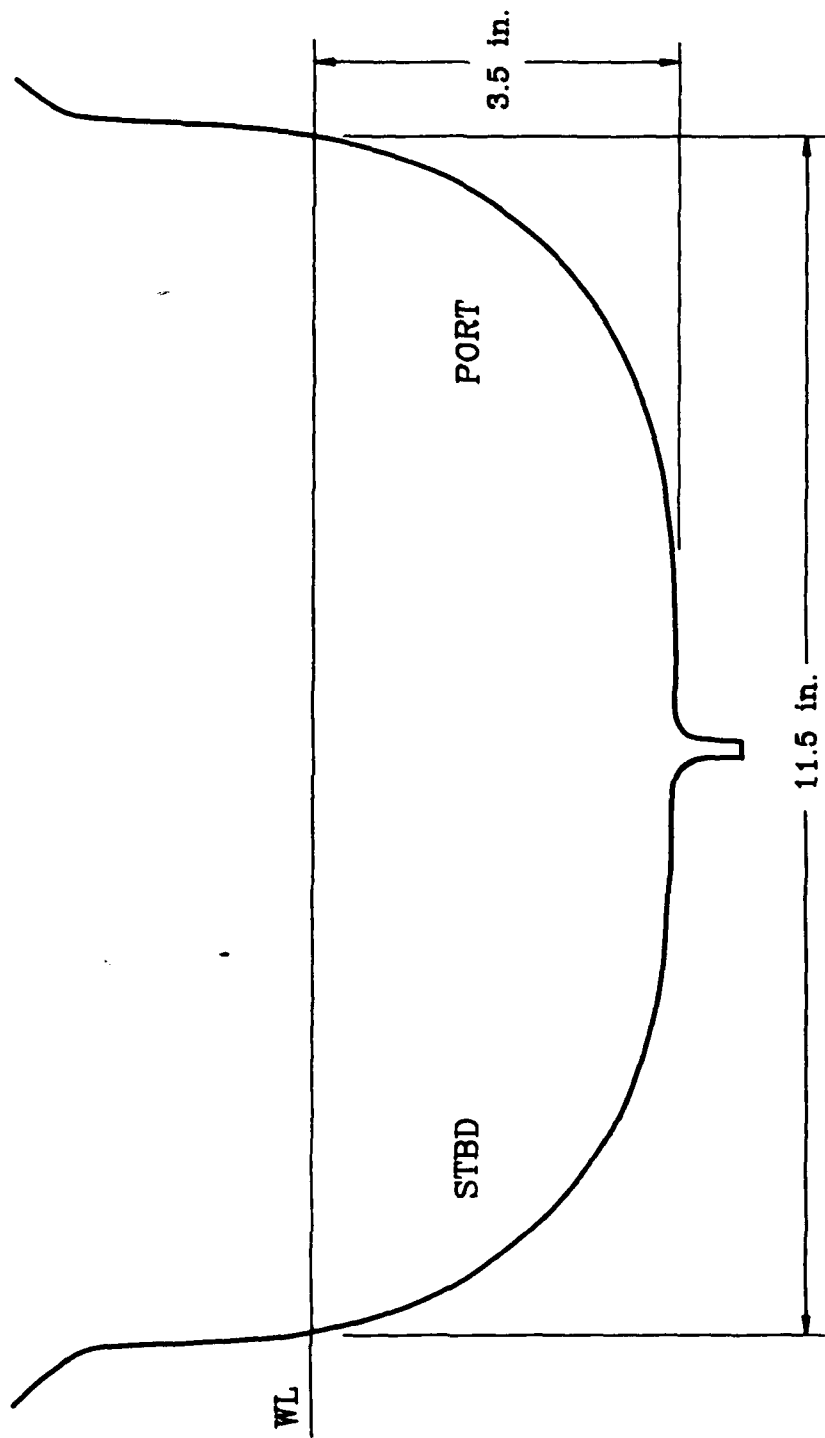


Figure 5. Model shape at $x = 14.5$ ft (4.42 m) from the forward perpendicular.

EXPERIMENTAL FLOW FACILITY

The experiment was conducted at the USNA 380 ft (116 m) basin. This basin is 26 ft (7.9 m) wide and 16 ft (4.9 m) deep, with photographic windows at mid-length. A complete description of the facility is given by Schroeder and Johnson (1972). The maximum carriage speed of 20 ft/s (6.1 m/s) is lower than was used in the ARL/PSU experiments. On this carriage it was possible to operate the air supply system manually and observe the wake and wave patterns near the model level visually.

The model was free to sink and trim. Towing hardware and instrumentation from previous rowing shell experiments by Coder et al. (1989) were used. The tow point was located 13.25 ft (4.04 m) from the FP and the sinkage measurement was made 13.54 ft (4.13 m) from the FP.

AIR JACKET

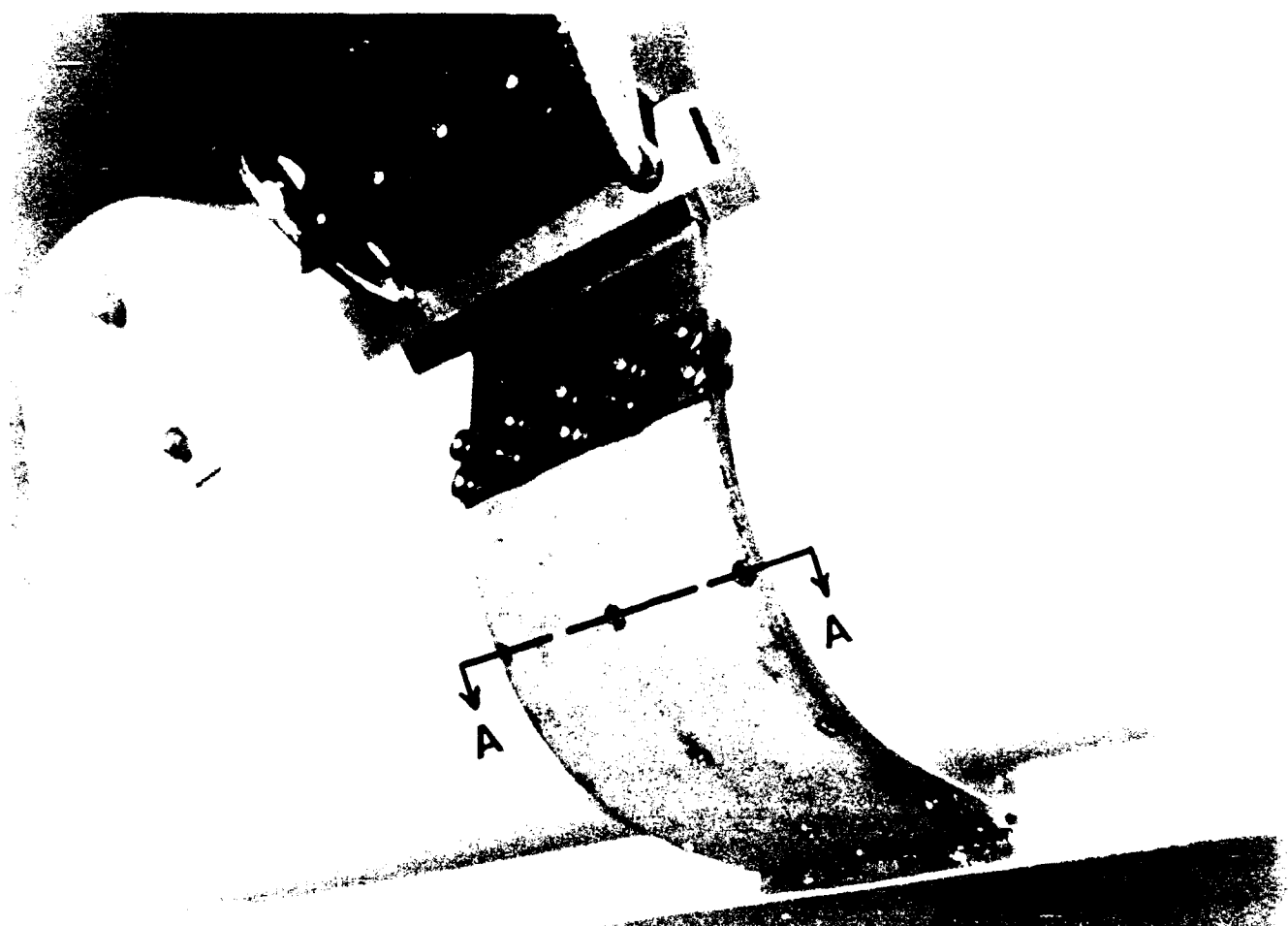
It was necessary to design the air jacket in a wraparound configuration, shown in Figure 6. In the ideal situation, it would be possible to cut the model skin to install the porous section flush-mounted, as was done in the ARL/PSU geometries. This would eliminate disturbance to the flowfield and allow installation of a plenum chamber behind the porous sections. However, this would have caused major structural damage to the shell, which was not acceptable since the shell was borrowed from the USNA Rowing Club.

A design analysis of the jacket was conducted to ensure that it would maintain its structural integrity and also not apply excessive loads to the rowing shell. An internal flow analysis was also conducted to insure uniform outflow distribution along the thin section. Generous fairings, approximately 5 in. (13 cm) long, were provided fore and aft of the air jacket to prevent flow separation. The fairings, constructed of wax, are visible in photographs

shown later in this report. The average fairing surface angle to the freestream was 3.6° , with a maximum angle of approximately 5° .

The streamwise length of the porous section was chosen at 4.25 in. (0.108 m) based on material availability and air flow rate considerations. Boundary layer thicknesses on the model were estimated as described in Appendix A. Using Eq. 3, a water flow rate Q_w of approximately 290 ft³/min or cfm (0.135 m³/s) was calculated for the highest towing speed of 20 ft/s (6.1 m/s). The nominal design air flow rate Q_a , using Eq. 2 with $Q_a/Q_w \approx 0.4$, was 120 cfm.

The design of the air jacket was conceived as a sandwich structure with a solid stainless steel backing or inner skin and a porous stainless steel outer skin. The lower ends of the two halves of the air jacket were fastened to the steering skeg through two common holes. As shown in Figure 6, the upper end of each half was clamped to the upper part of the shell structure. Two air gaps to allow flow around the entire circumference of the jacket were established by three spacers shown in the cross-section, Figure 7. A porous plate with a filtration grade of 10 μ m and a thickness of 0.062 in. (1.6 mm) was used. The solid backing plate was approximately the same thickness. A spacer thickness of 3/16 in. (4.8 mm) was chosen as a compromise between minimizing the total thickness of the air jacket and maximizing the structural strength and outflow distribution. Details of the air jacket design procedure and performance are given in Appendix B.



AIR SUPPLY SYSTEM

The air supply system was located on board the carriage. Air was supplied from four 30 gallon (0.11 m³) tanks which were charged to 135 psi (930 kPa) by a compressor during the return pass of the carriage. A filter was located between the compressor and the storage tanks. The tank manifold was connected through 30 ft of 1 in. I.D. hose to the metering and control board. The control elements consisted of a large ball valve for on/off and coarse adjustment, a regulating valve, and various gate valves. The total air flow passed through a 2-1/2 inch turbine meter and then was divided evenly into two legs by adjusting gate valves to equalize pressure gauge readings.

The air traveled from the control board, at the cabin level of the carriage, through twin 20 ft legs of 3/4 in. I.D. hose to manifolds mounted on the carriage structure above the model. Ten soft neoprene tubes (1/4 in. I.D.) were run to corresponding manifolds on the shell. The tubing had sufficient area to keep the velocity low and was flexible enough to prevent transmitting significant forces to the model. A rectangular piece of cardboard was mounted to the carriage immediately forward of the tubing to prevent wind drag on the tubing which would appear as a drag on the model. The air passed into 3/4 in. pipe, past a pressure transducer and a temperature transducer, and through 3 ft of hose to each side of the air jacket. Constant-area sheet-metal transition sections were constructed to connect 3/4 in. pipe to the highly elongated cross section of the air jacket.

PROCEDURES

The hull was ballasted, prior to model testing, to keep the same waterline as in previous bare hull experiments by Coder et al. (1989). The towing tank experiments were conducted during December 20-22, 1988, hereafter denoted "Days 1-3". Laboratory tests of the air jacket performance were subsequently performed and are discussed in Appendix B.

The manufacturer's flowmeter calibration was assumed correct. No corrections for temperature or pressure were made. At the highest air flow rate, a temperature decrease of about 1 °F (0.5°C) was observed during a complete discharge of the tanks. Because the air flow rate range achieved in the experiment was lower than expected, the meter was used well below its recommended minimum of 22 cfm. At the lower flow rates, some nonlinearity probably occurred. Overall uncertainty of the air flow rate is estimated at ±10 percent.

Model testing was performed as follows. The first series of tests was conducted with zero air flow rate. Subsequently, nominal air flow rate settings of 10, 20, 30 and 37 cfm were used through Day 2. Day 3 consisted of intermediate settings of 25, 15 and 5 cfm and finally another series at zero air flow rate. At each nominal air flow rate, a series of towing speeds ranging from 0 to 20 ft/s (6.1 m/s) was tested.

The zero-towing-speed measurements were recorded because of anticipation that buoyancy and tubing deflections might bias the drag readings. The small negative values of drag recorded at zero speed have been used to correct all forward-velocity drag measurements discussed in this report. The original, uncorrected data are listed in Appendix C.

The data truncation procedure was modified to include only steady air flow rate and steady drag load conditions. Coincidence of the two conditions for the maximum time interval was accomplished by opening the ball valve as the carriage accelerated. The resulting data-averaging times varied from approximately 4 s at 20 ft/s to 20 s at 4 ft/s.

DRAG MEASUREMENT UNCERTAINTY

Complete uncertainty analysis as it appears in the engineering literature is not usually applied to towing tank experiments. The first-order replication recommended by Coleman & Steele (1989) and others requires a large sample of runs to evaluate precision uncertainty. Obtaining this sample at, for example, only the highest and lowest towing speeds with one air flow rate would have consumed most of the available testing period. However, estimates from previous bare-hull tests, limited repeatability checks, and the consistent trends of the present data (while varying air flow rate and towing speed) all indicate small precision uncertainty for towing speeds above 4 ft/s. Furthermore, bias errors (e.g., due to gauge calibration factors) are not significant here since the results are mostly presented as ratios of measurements taken with identical instrumentation. This is consistent with the formal explanation by Coleman & Steele (1989) that correlated bias errors have a cancelling effect.

The drag measurement precision uncertainty is estimated (at a 95 percent confidence level) to be ± 2 percent at 8 ft/s and less than ± 2 percent at higher speeds. The largest precision errors are expected at the lowest speed of 4 ft/s for a linear gauge calibrated for speeds up to 20 ft/s (resulting in a force range of 20:1). The results to be shown at 4 ft/s indeed have large scatter and will be essentially disregarded.

RESULTS

TOTAL DRAG MEASUREMENTS

The results for zero air flow rate (the normalizing condition) and the maximum air flow rate are shown in Figure 8, where

$$C_T = \frac{R_T}{U_\infty^2 A_m \rho / 2} \quad (4)$$

$$R_n = \frac{U_\infty L}{v} \quad (5)$$

R_T is the total resistance, A_m and L are respectively the wetted area and length at zero speed, and ρ and v are the fluid properties. The freestream velocity U_∞ is closely approximated by the carriage towing speed. Repeat runs on Day 1 confirmed small precision uncertainty in the drag measurements. The normalized results are shown in Figure 9, grouped according to towing speed.

The zero-air-flow-rate results shown in Figure 8 differed between Day 1 and Day 3 by a significant amount relative to the total envelope of results. The discrepancy, which is greater than the precision uncertainty, may have been caused by physical alteration of the air jacket at the highest flow rate run at the end of Day 2 (see Appendix B for details).

Therefore, the C_T data taken chronologically up to that point were normalized with the Day 1 $C_{T,0}$ data, and the C_T data following that point were normalized with the Day 3 $C_{T,0}$ data.

The major result shown in Figure 9 is that no reduction in total drag was observed; in fact, total drag increased by up to 23 percent, with virtually all conditions showing some increase. The effect of air flow rate variations was much weaker than the effect of towing

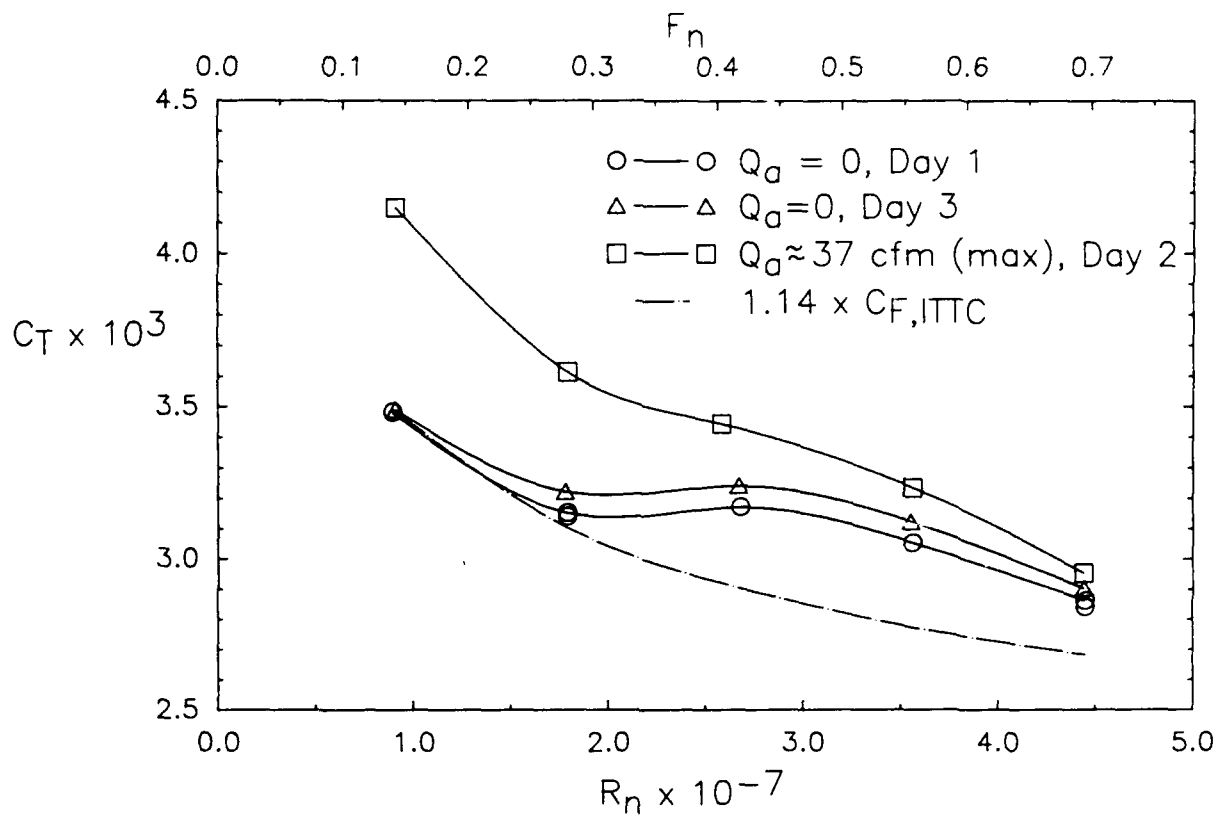


Figure 8. Shift in zero-air-flow-rate results relative to envelope of results.

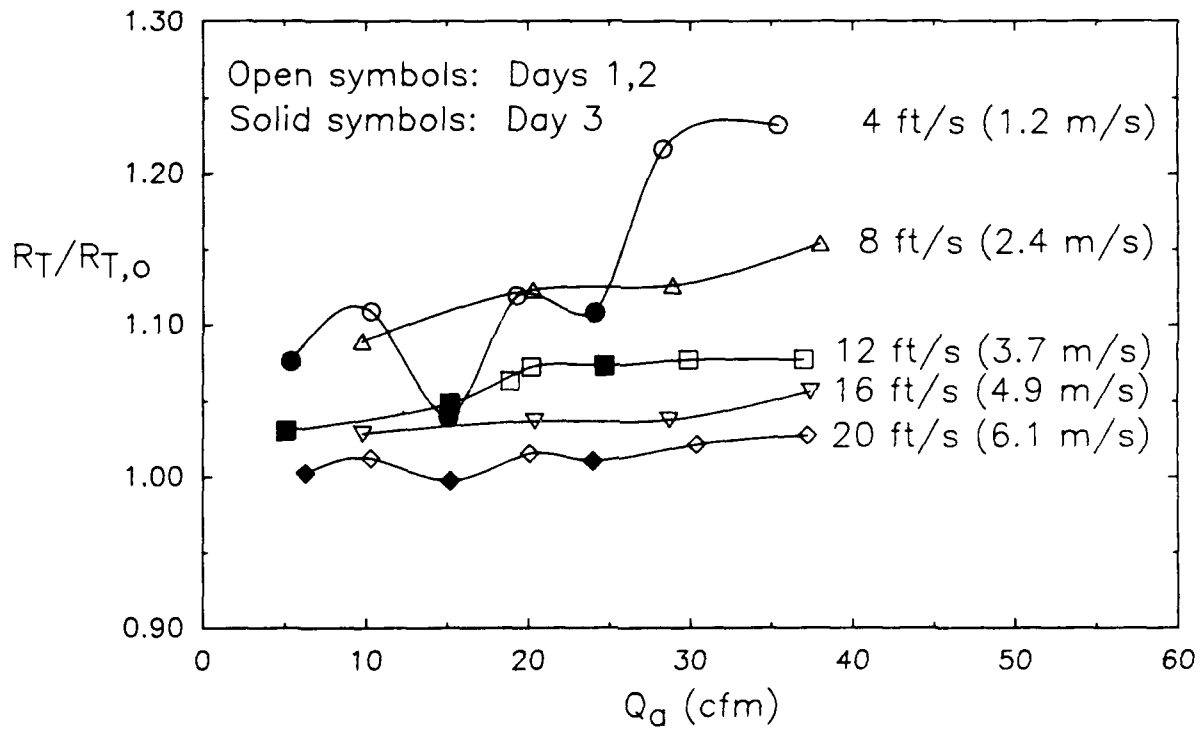


Figure 9. Results at all towing speeds and air flow rates.

speed variations. For a fixed nominal air flow rate, the drag ratio decreased and approached unity as the speed was increased.

Unfortunately, a maximum air flow rate of only about one third of the design value ($Q_a \approx 120$ cfm for $U_\infty = 20$ ft/s) was obtained. This was a result of the unexpectedly high pressure drop across the air jacket, which is discussed in detail in Appendix B.

VISUAL EVIDENCE

Figures 10 through 12 are photographs taken from the port side of the model, below the free surface, with the shell moving from right to left. A shutter speed of $1/250$ s was used. The photographs are aligned at left to the same reference point on the model; various downstream distances were captured according to the camera timing.

Figures 10a and 10b show runs with zero air flow rate. Figure 10a, chosen at low speed for maximum clarity, shows the wax fairings. Figure 10b, taken at the highest speed, shows the ventilation occurring on the air jacket. Some entrained air due to ventilation at the trip wire can also be seen at the bottom of the model. These effects were not noticed until a significant portion of the data had been accumulated.

At the lowest speed and highest air flow rate, shown in Figure 11, the air appears to have coalesced into very large bubbles. This condition is shown for general interest, although it is not expected to be representative of drag reducing conditions, since no small bubbles ("microbubbles") are present to modify the flow far downstream. The air volume in Figure 11 represents a dynamic phenomenon in which the air emerged from the jacket in a periodic fashion with a frequency on the order of 2 Hz. This was clearly observed with a mirror when holding the air jacket underwater. This phenomenon was also observed with porous metal plates tested between pipe flanges following the towing basin experiment. It is therefore

probably a result of cyclic capillary wetting and bubble shedding behavior rather than a resonance set up by the internal geometry of the air jacket.

A cloud of microbubbles appeared along the body only at the highest speeds and relatively low air flow rates (Figure 12b, c). For the conditions shown here, photographic coverage is not available to determine whether the bubble cloud persisted further downstream. Based on other photographs, it is unlikely that a large quantity of bubbles persisted for more than about 3 ft (0.9 m) aft of the air jacket for any conditions.

DRAG CHANGE DUE TO AIR EMISSION

The skin friction forward of the air jacket was presumably not modified by air emission. This component can therefore be subtracted from the data to more closely focus on drag changes aft of the air jacket. The wavemaking drag was another significant component of the measured total drag (Figure 8); as will be discussed later, this component may have been changed by air emission. However, for the simple analysis which follows, the zero-air-flow-rate wavemaking drag will be considered a tare which can be subtracted from the data.

The frictional drag forward of the air jacket can be estimated at all towing speeds using flat plate C_F correlations multiplied by a form factor. The form factor accounts for loss of pressure recovery due to finite thickness of the wake. It was found by "run-in" to the total drag data at the lowest Froude number, where wavemaking contributions should be negligible. Previous work by Coder et al. (1989) established a form factor of 1.04 for a similar bare model with the same tripping scheme. The Reynolds number was calculated using a wetted length of 14.5 ft to the air jacket, assuming the boundary layer virtual origin has been placed at the FP by use of the trip wire. C_F was then calculated from the ITTC correlation equation (Comstock, 1967). The area forward of the air jacket was 60 percent of the total wetted area.



Figure 10a. $U = 4$ ft/s, $Q_a = 0$ cfm.

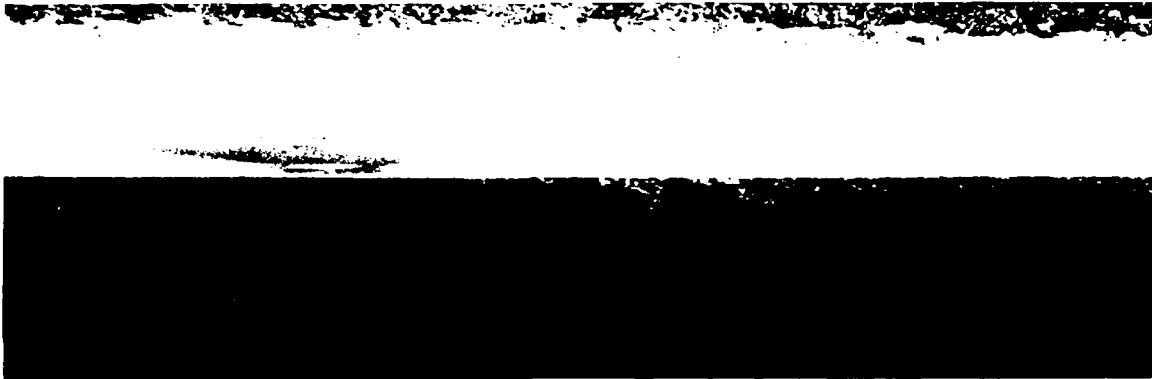


Figure 10b. $U = 20$ ft/s, $Q_a = 0$ cfm.

Figure 10. Zero air flow rate runs illustrating (a) wax fairing and (b) ventilation.



Figure 11. Low speed and high flow rate condition ($U = 4$ ft/s, $Q_a = 35$ cfm; $Q_a/Q_w = 0.52$).



Figure 12a. $U = 20$ ft/s, $Q_a = 37$ cfm ($Q_a/Q_w = 0.13$).

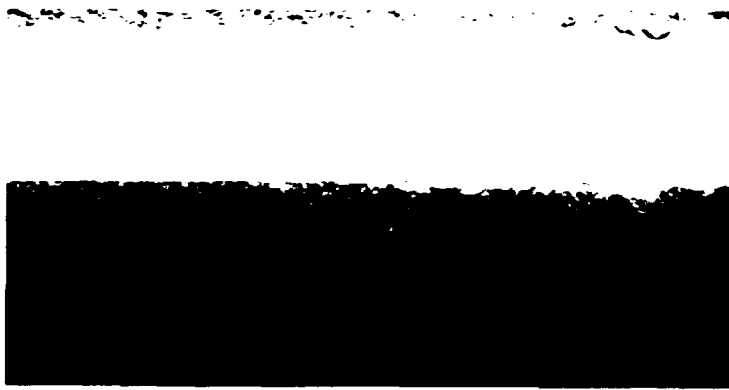


Figure 12b. $U = 20$ ft/s, $Q_a = 15$ cfm ($Q_a/Q_w = 0.05$).



Figure 12c. $U = 20$ ft/s, $Q_a = 5$ cfm ($Q_a/Q_w = 0.02$).

Figure 12. High speed runs.

It is assumed that the wetted area was not significantly changed by air emission. The model was free to sink and trim about the towing point, but the area covered by air emission was not symmetric about the tow point. Rough analysis of the sinkage and trim data indicated that significant changes in wetted area probably did not occur upstream or downstream of the air jacket. A more refined analysis would also account for changes in wetted area and pressure distribution due to ventilation of the trip wire and the air jacket. However, such analysis would require knowledge of the actual waterline profile resulting from the surface waves.

The wavemaking drag at $Q_a=0$ was calculated as the difference in the measured total drag and the estimated frictional drag, following the standard naval architecture analysis. The form factor for the entire model was 1.14, as shown in Figure 8. This relatively high form factor compared to the bare model case is attributed to the presence of the air jacket. Figure 8 indicates wavemaking drag becoming significant in the middle range of Froude numbers of the present experiment. Recent detailed measurements on a similar rowing shell at DTRC* confirm that wavemaking drag has its maximum contribution at $F_n = 0.45$.

Figure 13 shows the result of subtracting the two drag components discussed above. The remaining drag component, denoted C_{AFT} , is the frictional drag aft of the air jacket combined with possible changes in form drag and wave drag. Further isolation of the drag contributions would require local measurements on the model and in the towing basin. The 4 ft/s (1.2 m/s) runs are not included in Figure 13, since at this speed the uncertainties are large and the photographs indicate that microbubbles are not created, even at the lowest air flow rates. As expected, the drag increases shown are much larger than estimated earlier using the entire model drag.

*Unpublished resistance and wave cut measurements by P.A. Chang (1989).

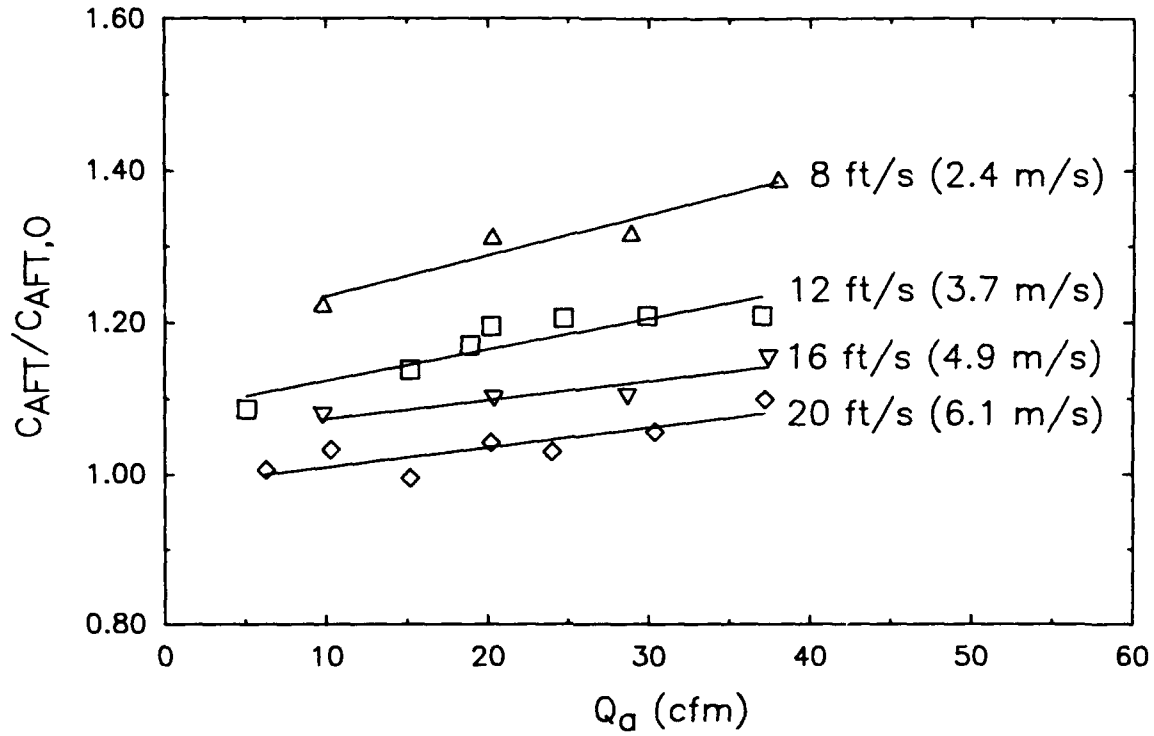


Figure 13. Estimated effect on drag aft of air jacket.

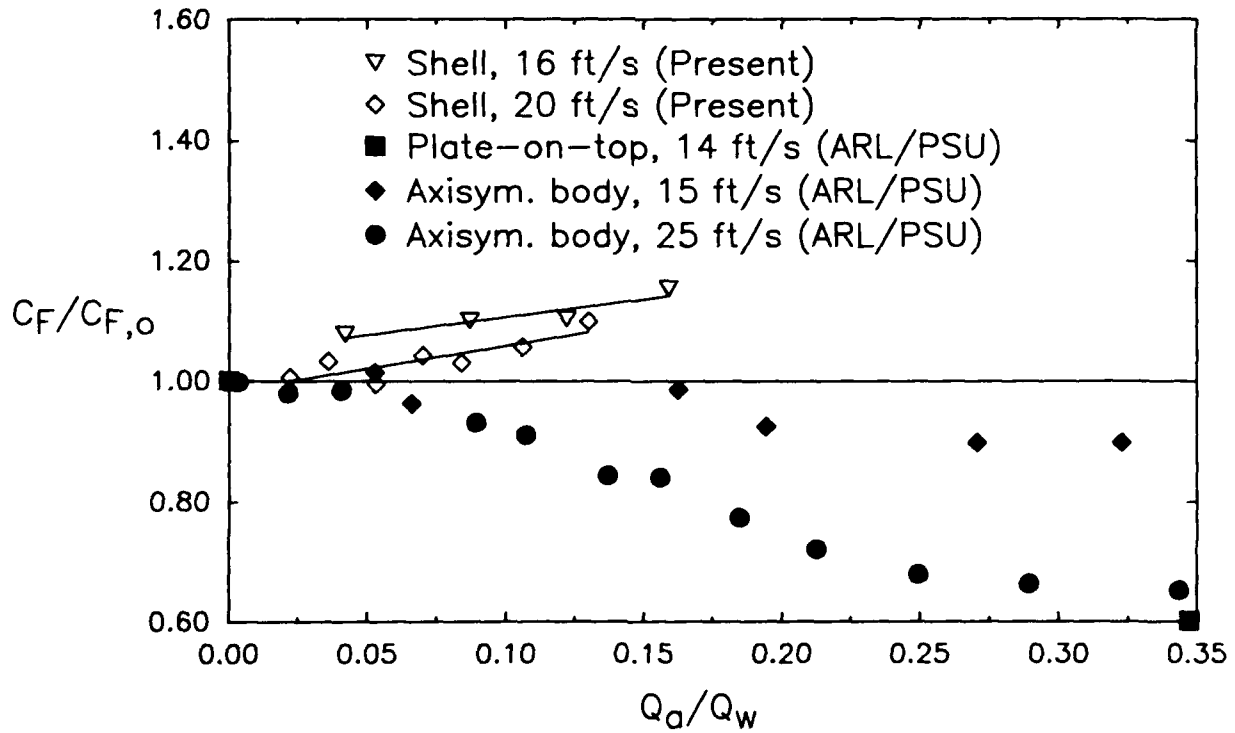


Figure 14. Rough comparison with ARL/PSU data.

DISCUSSION

SPEED DEPENDENCE

The ARL/PSU data on which projections of performance were based corresponded to instances where buoyant confinement or high speeds maintained bubbles in the boundary layer. The present results, representing partial buoyant confinement by geometry, deviated most strongly at low speeds and showed a trend toward lower drag as the speed increased to the maximum carriage speed. However, because the intervals between lines of constant speed became progressively smaller as the speed was increased, there was no strong indication that drag reduction would have occurred at higher speeds. Cross-plotting the data from Figure 9 versus velocity for nominally constant air flow rate verified this.

Furthermore, it is desirable to operate a surface ship model at low, Froude-scaled speeds to prevent ventilation, unrealistic sinkage and trim, and planing. Thus, the importance of buoyancy in experiments with air emission (i.e. the apparent requirement of high absolute speeds) is in conflict with the Froude scaling approach. This conclusion implies, unfortunately, that model scale experiments do not determine whether the microbubble drag reduction method is applicable to surface ships.

COMPARISON WITH ARL/PSU RESULTS

Additional insight into the lack of drag reduction in the present results has been sought by more exactly comparing the present experimental parameters with the ARL/PSU data. Data from the two highest speeds shown in Figure 13 are plotted in Figure 14 along with the ARL/PSU data at comparable speeds. All air flow rates have been normalized as in Eq. 2. For the range of parameters shown, only one datum, $Q_g/Q_w=0.345$, is available from the ARL/PSU flat plate experiments.

The axisymmetric body data indicate a strong speed dependence in this speed range due to the effect of buoyancy on the air bubbles. Deutsch & Pal (1990) have recently shown that a double vortex structure, presumably caused by a gravitational instability, occurs on the axisymmetric body at 15 ft/s. This structure is accompanied by local increases in skin friction, resulting in small overall skin friction reduction. Similar results occur at 25 ft/s but at higher air flow rates. The effect of buoyancy is expected to be magnified if the bubbles coalesce as they are swept along a longer body such as used in the present study. At the highest speed and lowest air flow rate, shown in Figure 12c, few bubbles remain after about 10 in. (0.25 m) from the trailing edge of the air jacket; this was also the condition which illustrated the smallest drag increase (Figure 9).

Because of the high pressure drop across the air jacket, the maximum Q_a/Q_w achieved in the present experiment (at the higher speeds shown in Figure 14) was 0.16. This would indicate at most approximately 20 percent C_F reduction based on the ARL/PSU results. For the conditions in which microbubbles were observed on the rowing shell (Figures 12b, c), the low Q_a/Q_w values indicate negligible C_F reduction. On the other hand, the trend of the present results is unfavorable; no drag reduction can be predicted at higher air flow rates. It should also be noted that the air flow rate scaling method used here, if applicable, will predict very high air flow rate requirements for the thick boundary layers on naval vessels. The resulting high pressures may require a stronger porous material than used in the present experiment.

A reviewer has suggested that the shear stress magnitude on the rowing shell is inadequate for creation of microbubbles. However, the shear velocity estimated at the air jacket is close to the values given near the ARL/PSU porous sections (Madavan, 1984; Deutsch & Castano, 1986) for a similar speed of 16 ft/s (≈ 5 m/s).

Removal of bubbles from the region of the boundary layer nearest the hull is caused by turbulent diffusion, in addition to the buoyancy effect already discussed. The importance of diffusion in diluting the injected fluid has been established for polymer drag reduction (e.g., Latta & El Reidy, 1976), leading to suggestions that the injection on a long, high-speed body be done at several streamwise stations. A similar scheme may be required to achieve drag reduction with microbubbles on bodies longer than those tested at ARL/PSU.

POSSIBLE MECHANISMS CAUSING DRAG INCREASES

After subtraction of the obvious extraneous drag effects, the present data have a trend (Figure 14) opposite to that of the ARL/PSU data. This contrast indicates different phenomena probably occurred in the present experiment than in the ARL/PSU experiments. The authors have considered several hypotheses which could account for drag increases, possibly masking any reductions in skin friction.

Tasaki et al. (1975) showed that air bubbles clinging to the skin of a surface model can increase the apparent frictional resistance. This was demonstrated for models towed at 3 to 4 ft/s. As bubbles collected on the surface of a model over a period of time, apparent frictional drag increases of approximately 20 percent were measured. However, Tasaki et al. stated that the problem was more severe for full ship forms at low speed than fine ones at high speed. This effect would also be expected to appear intermittently. The consistent trends evident in the present data indicate that bubble adhesion was not a significant factor.

All of the ARL/PSU experiments were done on submerged bodies. It is possible that significant wavemaking drag increases occurred when air was emitted from the present model. Wave resistance calculations based on wave cut measurements would help confirm this possibility. Analysis or computation might also be done by representing the air emitted as an

additional potential flow "source". Plotting the present experimental results versus Froude number, for the relatively coarse matrix of F_n tested, indicates no distinct trends.

Finally, boundary layer thickening and separation are possible causes of form drag increases. Deutsch & Clark (1990) have recently observed separation in a microbubble-modified boundary layer with an adverse pressure gradient. The present fairing length was considered to be adequate for the Newtonian (water only) flow. However, injection of air would reduce the momentum in the boundary layer near the wall, making the boundary layer more susceptible to separation on the aft side of the air jacket fairing. A similar argument is commonly given (e.g., Fox & McDonald, 1978) when comparing laminar and turbulent boundary layers in the context of separation. For a given air flow rate, the extent of the separated region would be expected to decrease as the towing speed is increased. The total drag ratio would then decrease as the speed is increased, consistent with the trend shown in Figure 9.

CONCLUSIONS

1. Drag reduction using localized air emission from a long, slender hull does not appear to be possible at low absolute speeds, due to the influence of buoyancy. The apparent requirement of high speed leads to difficulties in model-scale testing for surface ships.
2. Emission from several longitudinal stations will probably be required to overcome loss of bubbles by buoyancy and diffusion and to minimize local flow disturbance.
3. The governing parameter for microbubble drag reduction in most of the ARL/PSU configurations is the ratio of injected air flow to the water flow rate in the boundary layer. This parameter is applicable for air microbubbles confined to the boundary layer either by buoyancy (body geometry) or high speeds. It is not clear that the same parameter will

correctly scale up air flow rate requirements for higher Reynolds numbers on arbitrary geometries.

4. An air jacket configuration, while convenient for retro-fit applications, may cause separation of a boundary layer filled with bubbles and may fail to reduce drag.

RECOMMENDATIONS

1. Future experiments with air emission through porous surfaces should use only flush-mounted areas in the hull. The pressure distribution on the afterbody should be measured to detect the presence of separated flow regions.

2. In further experiments, emission from several stations along the hull should be considered.

3. For experiments on surface ship models in which the boundary layer is strongly modified, wave-cut measurements should be done to allow isolation of the wave drag component.

4. The high pressure drop encountered in the present experiment indicates that a candidate emitter geometry should be tested prior to model testing, using realistic porous metal type and immersion conditions.

ACKNOWLEDGMENTS

This work was aided by J. Hill, S. Enzanger, and D. Bunker of the USNA Hydromechanics Laboratory and T. Price from the USNA Woodworking Shop. Midshipman and Trident Scholar D.B. Walker (now ENS, USN) participated in the experimental design, preparation, and measurements. C.L. Merkle and S. Deutsch of ARL/PSU provided helpful comments concerning interpretation of the results. At DTRC, J.A. Bradel performed a finite element structural analysis of the air jacket. The Sheet Metal and Welding Shops and the East End Fitting Room gave expert and timely assistance. B.B. Wisler assisted with the experiment preparation. H.G. Strunk and J.N. Blanton assisted in the data collection. M.A. Jones performed the photography. T.A. Berwick and S.L. Thompson conducted followup testing of the porous metal as part of the DTRC Summer Engineering Apprentice Program. Finally, the authors acknowledge insightful comments made by W.R. Lindenmuth in his review of this report.

APPENDIX A

BOUNDARY LAYER FLOW RATE ESTIMATES

Estimates of the boundary layer 99 percent velocity thickness δ and displacement thickness δ^* are required in Eq. 3 to compute Q_w . Textbook flat-plate correlations are not expected to apply exactly to the boundary layers of interest here due to the influence of trip wires and pressure gradients. The quantity δ is of primary concern since it is approximately an order of magnitude larger than δ^* . A two-dimensional analysis was maintained by substituting respectively the circumference of the ARL/PSU axisymmetric body and the girth of the present body for the spanwise width, b , in Eq. 3. This approximation is valid because in each case δ is much smaller than the body radius.

The ARL/PSU papers do not report δ and δ^* measurements at the midpoint of the porous sections and at all freestream velocities of interest. Extrapolations from the data given were required. The present experiment was a more difficult situation since no velocity profiles were measured on the body.

ARL/PSU FLAT PLATE EXPERIMENTS

Madavan (1984) measured velocity profiles at $x_{LE} = 0.092, 0.194, \text{ and } 0.274$ m from the leading edge (LE) of the porous section for freestream velocities of 4.7 and 10.5 m/s. The middle of the porous section was nominally the same ($x_{LE} = 0.089$ m) location as the first measurement station. From the velocity profiles plotted by Madavan, it can be deduced that $\delta/\delta^* \approx 8$, consistent with the flat plate correlations given by White (1974). Madavan also provided a table of δ^* and θ values. For the present work, least-squares regression was performed to predict $(\delta - \delta^*) \approx 7\delta^*$ at $x_{LE} = 0.089$ m over the full range of freestream velocities for the flat plate experiment. The regression equation chosen was

$$Re_{\delta^*} = \frac{U_{\infty} \delta^*}{\nu} = A \left[\frac{U_{\infty}(x_{LE}+C)}{\nu} \right]^B \quad (6)$$

where C is the distance from a virtual origin of turbulence to LE. Equation 6 is equivalent to the classical power-law correlations given by Schlichting (1979) and White (1974) when their values of the exponent B are used. Unlike the classical flat-plate experiments, the ARL/PSU measurements were made on the wall of the water tunnel in which the boundary layer apparently originated in the contraction section. Regression on the six data points (U_{∞} , x_{LE} , δ^*) and $\nu = 0.985 \times 10^{-6} \text{ m}^2/\text{s}$ provided by Madavan gives a good fit to

$$Re_{\delta - \delta^*} = 0.0544 \left[\frac{U_{\infty} (x_{LE} + 0.247\text{m})}{\nu} \right]^{0.9246} \quad (7)$$

Predictions from Eq. 7, presented in Table A1, were applied to the ARL/PSU results shown in Figure 1 to obtain Figure 3. Because of the approximate nature of the analysis, the final result (Q_w estimate) is given to only two significant figures.

Table A1. Q_w estimates at $x_{LE} = 0.089 \text{ m}$.

U_{∞} (m/s)	$Re_x \times 10^{-6}$	$\delta - \delta^*$ (mm)	$Q_w \times 10^3$ (m^3/s)
4.2	1.43	6.28	2.7
9.3	3.17	5.91	5.6
12.4	4.23	5.79	7.3
17.4	5.94	5.64	10.

ARL/PSU AXISYMMETRIC BODY EXPERIMENT

Deutsch & Castano (1986) used a trip wire at $x = 0.046$ m from the nose of the body. Re_θ values were reported at $x_{TW} = 0.155, 0.277,$ and 0.403 m from the trip wire. The porous section was located at $x_{TW} = 0.1005$ m, well upstream of the first measurement station. The nine data points ($U_\infty, x_{TW}, Re_\theta$) can be represented fairly well by a power law similar to Eq. 6. The classical shape factor $\delta^*/\theta \approx 1.27$ can then be used to obtain

$$Re_{\delta^*} = 0.00114 \left[\frac{U_\infty(x_{TW}+0.275\text{m})}{v} \right]^{1.0145} \quad (8)$$

The value of v used by Madavan (1984) in the same water tunnel was used here. Deutsch* has provided the authors with δ values computed from measured velocity profiles at the same x stations. A good fit is given by

$$Re_\delta = 0.00159 \left[\frac{U_\infty(x_{TW}+0.275\text{m})}{v} \right]^{1.1093} \quad (9)$$

The estimates presented in Table A2 were applied to Figure 2 to obtain Figure 4.

Table A2. Q_w estimates at $x_{TW} = 0.1005$ m.

U_∞ (m/s)	$Re_x \times 10^{-6}$	$\delta - \delta^*$ (mm)	$Q_w \times 10^3$ (m ³ /s)
4.6	1.75	2.35	3.0
7.6	2.91	2.53	5.4
10.7	4.10	2.64	7.9
16.8	6.40	2.78	13.

*Personal communication with S. Deutsch, ARL/PSU, State College, Pennsylvania (1990).

PRESENT EXPERIMENT

The present experiment had higher Re_x at the porous metal location than the ARL/PSU experiments. The relationship given by Granville (1959) was chosen:

$$\frac{\delta}{x} = \frac{0.0598}{\log_{10} Re_x - 3.170} \quad (10)$$

Souders (1974) stated that this equation was fairly consistent with full scale measurements at $Re_x = 1.2-2.5 \times 10^8$ on a submarine. It is also consistent with a single value of δ reported by Klebanoff (1954) for his wind tunnel flat plate experiment at $Re_x = 4.2 \times 10^6$. The relationship $\delta^*/\delta = 0.129$ from the correlations given by White (1974) was assumed to hold for the boundary layer on the rowing shell.

Because no velocity profiles were measured on the rowing shell, the virtual origin could not be empirically determined. The boundary layer thickness is expected to be strongly affected by the trip wire and the ventilated area downstream of the trip wire. As a first approximation, the virtual origin was assumed to be at the forward perpendicular. Using a wetted girth of 1.33 ft, Q_w estimates then follow as shown in Table A3.

Table A3. Q_w estimates at $x_{FP} = 14.5$ ft.

U_∞ (ft/s)	$Re_x \times 10^{-6}$	$\delta - \delta^*$ (ft)	$\delta - \delta^*$ (mm)	$Q_w \times 10^3$ (cfm)
4.0	5.07	0.213	65	69
8.0	10.1	0.196	60	125
12.0	15.2	0.188	57	180
16.0	20.3	0.182	55	235
20.0	25.4	0.178	54	290

APPENDIX B

AIR JACKET PERFORMANCE

A good design, providing a well-distributed outflow along the air jacket, has high outflow resistance relative to the internal resistance along the air gap channels. A literature review found no previous studies of parallel-plate turbulent channel flows with the inlet flow exhausted through one wall. An approximate analysis of the outflow uniformity was done using the air jacket geometry as described earlier and the manufacturer's pressure drop data (Mott, 1988) for air flowing through porous metal plates, shown as the lower dashed line in Figure B1. All data in Figure B1 are for porous stainless steel plates with a filtration grade of 10 μm . The analysis indicated an outflow per unit area decreasing by only about 10 percent from the waterline to the skeg. Structural analysis of the design indicated acceptable stresses and deflections. However, the structural analysis assumed a much smaller screw spacing than was used in the final construction. More importantly, the pressure drop prediction used in the flow distribution analysis and the structural analysis was experimentally found to be unrealistically low.

The air jacket was connected to the air supply system on shore for preliminary testing. The pressures were relatively low, on the order of 1 psi (7 kPa), as expected from the Mott (1988) data for air-into-air. However, upon immersion the back pressure became much larger; this persisted for some time after the air jacket was removed from the water. Similarly high levels of pressure drop were encountered during the rowing shell tests as shown in Figure B1. Data from the dissertation by Madavan (1984) which became available after the experiment are also included in the figure.

The resistance of the porous metal in the present experiment is approximated using the back pressure or gauge pressure at the transducer location. The assumption of negligible flow

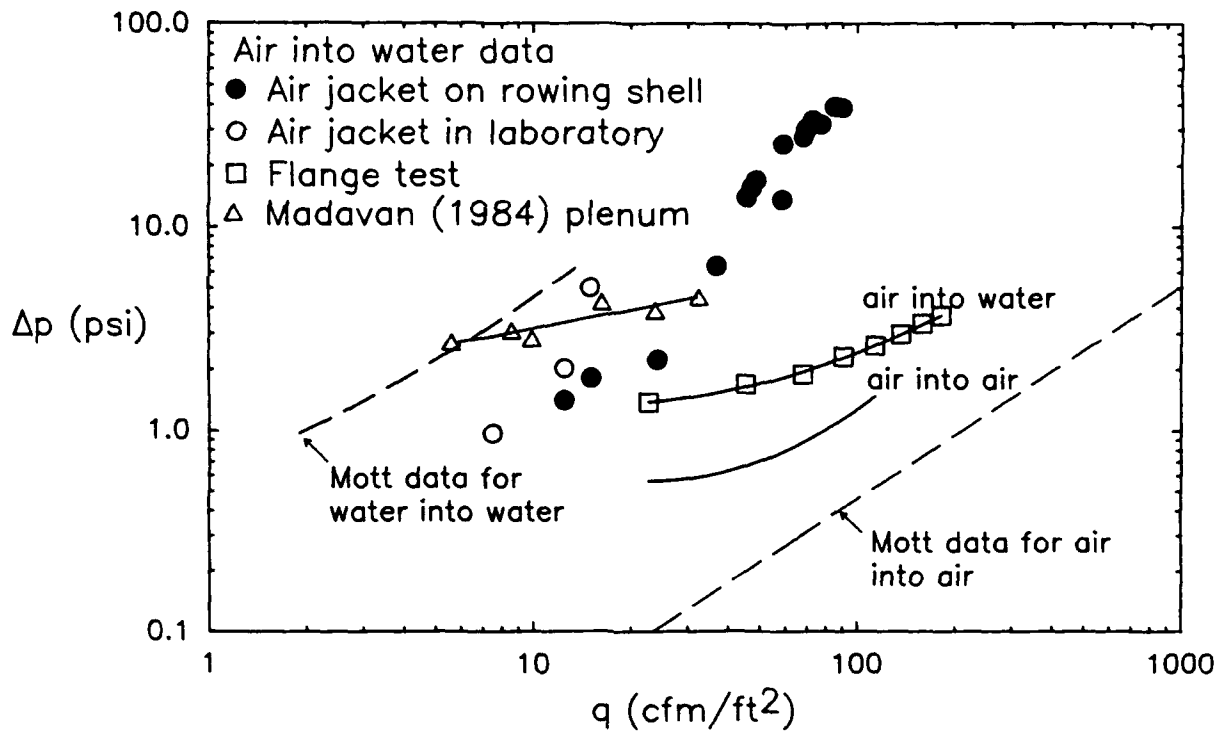


Figure B1. Pressure drop of 10 μm porous metal configurations.

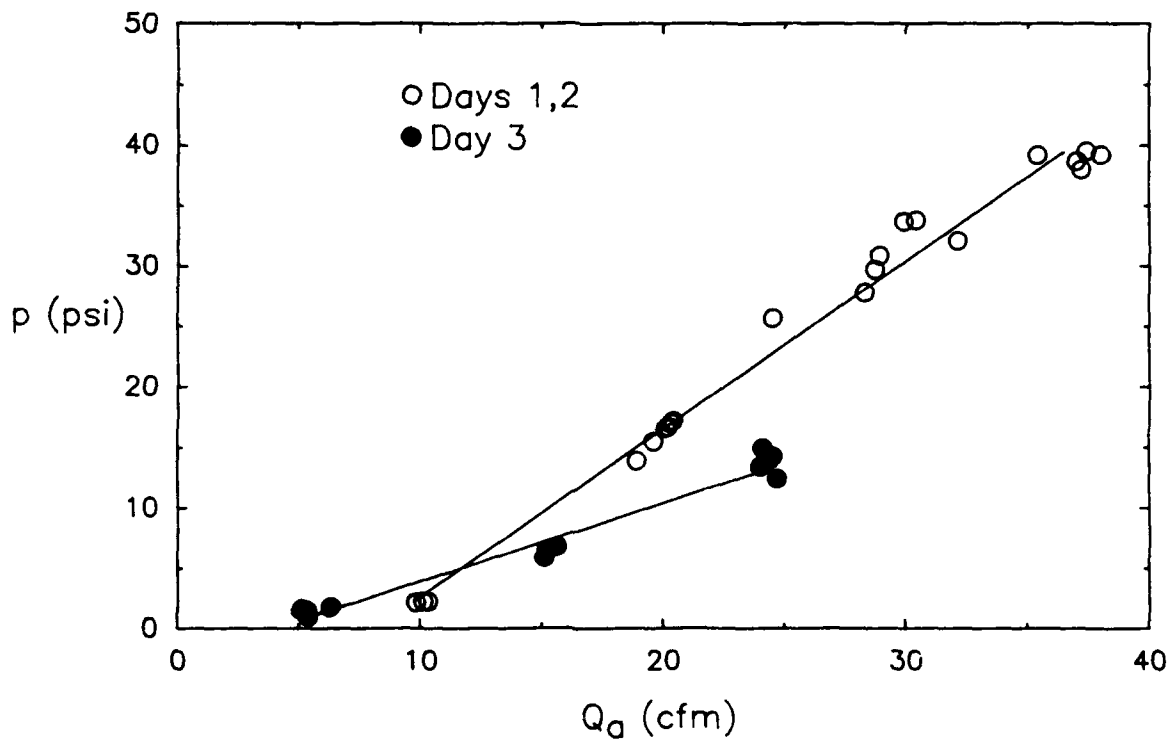


Figure B2. Details of air jacket air flow resistance.

resistance in the hose, fittings, and shape transition section is verified by the low back pressure of the dry onshore tests. A laboratory test was also done several months later with the starboard half of the air jacket immersed and a pressure transducer installed immediately upstream of the transition section. The slope of these data, shown in Figure B1, is consistent with the data from the rowing shell tests.

Further tests were performed with small porous metal plates held between pipe flanges. The latter arrangement is a more pure measure of porous plate resistance and a closer simulation of the Madavan (1984) experiment which used a plenum chamber behind the plate. The porous metal samples used were obtained from the same manufacturer and had identical specifications to the plate used to construct the air jacket. As shown in Figure B1, the measurements for air into water have a slope more consistent with the Madavan data than with the air jacket data. The data for air into air indicate a pressure drop approximately 1 psi lower. Surface tension acting on the air as bubbles are created on the water side is sufficient to explain a pressure increase of this order. It is also likely that cyclic capillary wetting occurred in the air into water case (see Visual Evidence). This would increase the mean pressure drop significantly over the air into air case. However, the uniquely large resistance of the air jacket, relative to the Madavan configuration, is apparently due to an interaction of the immersion condition with the narrow-channel internal flow geometry of the air jacket.

The present experiment design air flow rate, if achieved, would have produced an air flux (as on the abscissa of Figure B1) of approximately 300. This is significantly higher than in the ARL/PSU experiments due to the thicker boundary layer on the present model. Potential higher-Reynolds number applications are expected to be a severe test of the porous metal resistance and strength characteristics. It is also interesting to note that Madavan's other data (not shown here) indicate no significant difference in pressure drop for filtration

grades of 10 and 100 μm . This implies that air pumping power requirements with sintered metal plates cannot be significantly reduced by using larger pore sizes.

The unanticipated high pressure drop had several effects on the experiment. Because the supply pressure was fixed, the achievable flow rate was reduced to approximately 40 cfm compared to the design flow rate of 120 cfm. This resulted in the flowmeter being used below its recommended range. One beneficial effect of higher resistance is a better flow distribution than predicted in the design analysis. Not only is the outflow resistance higher, but the internal resistance should be greatly decreased by the reduced flow rate. When the air jacket was observed with mirrors from the lower carriage platform, the air appeared to be emerging uniformly from the full girth of the model.

A major effect of the high pressures (up to 40 psi at the highest flow rate) was a high structural load on the air jacket. To examine the possibility that the high loads may have damaged the air jacket, the air jacket resistance data are shown separated by testing days in Figure B2. The air flow rate was gradually increased on Days 1 and 2. When the highest flow rate was reached, a whistling tone was heard in the area of the air jacket. Various connections were checked and tightened, to no avail. Intermediate flow rates were tested on Day 3, as shown in Figure B2, to complete the experimental matrix. From the trends shown in this figure, it appears that the total resistance of the air jacket (the quantity actually measured by the pressure transducer) was different for Day 3 compared to Days 1 and 2. This is possibly due to a failure in the silicone sealant, or buckling of the porous metal, between the screws which secured the outer skin of the air jacket.

APPENDIX C

DATA

Day	Time	Tow speed (ft/s)	Drag (lbf)	Trim (°)	Sinkage (ft)	Air flow rate (cfm)
1	1017	0.000	0.006	—	-0.060	0.0
1	1026	4.009	1.428	—	-0.051	0.0
1	1038	8.010	5.146	—	-0.167	0.0
1	1048	8.017	5.139	—	-0.141	0.0
1	1059	12.008	11.634	—	-0.307	0.0
1	1109	15.962	19.767	—	-0.375	0.0
1	1126	19.930	28.869	0.483	-0.320	0.0
1	1148	19.940	28.731	0.479	-0.349	0.0
1	1357	0.000	0.000	-0.006	0.025	10.1
1	1410	4.071	1.584	-0.007	-0.009	10.3
1	1422	8.045	5.592	0.004	-0.110	9.8
1	1453	15.993	20.317	0.385	-0.420	9.8
1	1507	20.016	29.146	0.484	-0.276	10.3
1	1546	11.989	12.320	0.175	-0.306	18.9
1	1558	0.000	-0.037	-0.015	0.012	19.6
2	0835	0.000	-0.048	-0.004	0.020	19.5
2	0853	3.984	1.537	-0.005	-0.052	19.3
2	0914	8.056	5.723	0.006	-0.122	20.3
2	0929	11.982	12.415	0.174	-0.240	20.2
2	0940	15.893	20.424	0.364	-0.360	20.4
2	0953	19.981	29.190	0.462	-0.277	20.1
2	1040	0.000	-0.087	-0.009	0.052	24.5
2	1051	4.072	1.636	0.003	-0.097	28.3
2	1107	7.975	5.695	-0.002	-0.138	28.9
2	1125	11.990	12.435	0.171	-0.280	29.9
2	1142	15.883	20.408	0.365	-0.352	28.7
2	1315	19.986	29.306	0.445	-0.215	30.4
2	1345	0.000	-0.099	-0.015	0.074	32.1
2	1420	4.067	1.647	0.003	-0.044	35.4
2	1440	8.036	5.826	-0.001	-0.168	38.0
2	1500	11.964	12.426	0.167	-0.261	37.0
2	1518	15.947	20.761	0.329	-0.293	37.4
2	1530	19.882	29.488	0.472	-0.220	37.2

Day	Time	Tow speed (ft/s)	Drag (lbf)	Trim (°)	Sinkage (ft)	Air flow rate (cfm)
3	0828	4.021	1.560	-0.006	-0.027	24.1
3	0858	12.006	12.604	0.183	-0.268	24.7
3	0917	20.007	29.476	0.493	-0.301	24.0
3	0932	4.067	1.523	-0.009	-0.034	15.1
3	0949	11.967	12.374	0.186	-0.294	15.2
3	1005	19.996	29.114	0.516	-0.357	15.2
3	1023	4.075	1.567	-0.005	-0.072	5.4
3	1036	11.966	12.143	0.177	-0.205	5.1
3	1052	19.886	29.223	0.484	-0.266	6.3
3	1130	0.000	-0.004	0.007	-0.066	15.6
3	1145	0.000	-0.014	-0.006	0.066	5.3
3	1315	0.000	0.006	0.000	-0.028	0.0
3	1331	4.072	1.476	0.000	-0.016	0.0
3	1343	7.979	5.219	0.012	-0.129	0.0
3	1355	11.973	11.807	0.184	-0.249	0.0
3	1434	15.889	20.043	0.375	-0.387	0.0
3	1445	19.887	29.193	0.528	-0.258	0.0
3	1458	0.000	-0.069	-0.012	0.094	24.5

Water temperature = 65 °F; $\nu = 1.14 \times 10^{-5}$ ft²/s from Comstock (1967)

REFERENCES

- Bogdevich, V.G., Evseev, A.R., Malyuga, A.G. & Migirenko, G.S. 1977 Gas-saturation effect on near-wall turbulence characteristics. Second International Conference on Drag Reduction, Cambridge, England, Paper D2. BHRA Fluid Engineering.
- Brown, D.A. 1990 Attempts to achieve drag reduction via electrochemically produced microbubbles. Proceedings of the Second International Symposium on Performance Enhancement for Marine Applications, pp. 219-226. Newport, Rhode Island.
- Canham, H.J.S., Catchpole, J.P. & Long, R.F. 1971 Boundary layer additives to reduce ship resistance. The Naval Architect, July, pp. 187-213.
- Coder, D.W., Walker, D.B., McKelvey, D.J. & Enzinger, S.W. 1989 Drag reduction with riblets on rowing shells. Presented at 22nd ATTC, St. John's, Newfoundland.
- Coleman, H.W. & Steele, W.G. 1989 Experimentation and Uncertainty Analysis for Engineers, Wiley-Interscience.
- Comstock, J.P. (ed.) 1967 Principles of Naval Architecture, published by The Society of Naval Architects and Marine Engineers.
- Deutsch, S. & Castano, J. 1986 Microbubble skin friction reduction on an axisymmetric body. Physics of Fluids **29**, pp. 3590-3597.
- Deutsch, S. & Clark, H. 1990 Microbubble drag reduction in an axial pressure gradient. Bulletin of the American Physical Society **35**, abstracts for 43rd Annual Meeting of the Fluid Dynamics Division, p. 2233.
- Deutsch, S. & Pal, S. 1990 Local shear stress measurements on an axisymmetric body in a microbubble modified flow field. Physics of Fluids A **2**, pp. 2140-2146.
- Fox, R.W. & McDonald, A.T. 1978 Introduction to Fluid Mechanics, 2nd ed., John Wiley & Sons, pp. 419-420.
- Granville, P. 1959 The determination of the local skin friction and the thickness of turbulent boundary layers from the velocity similarity laws. International Shipbuilding Progress **7**, No. 69, May, 1960, pp. 213-220.
- Hoyt, J.W. 1972 The effect of additives on fluid friction. Trans. ASME Journal of Basic Engineering, June, pp. 258-285.
- Klebanoff, P.S. 1954 Characteristics of turbulence in a boundary layer with zero pressure gradient. 41st Annual Report of NACA, Report 1247 (also NACA TN 3179).
- Latto, L. & El Reidy, O.K.F. 1976 Diffusion of polymer additives in a developing turbulent boundary layer. Journal of Hydronautics **10**, No. 4, pp. 135-139.
- Madavan, N.K. 1984 The effects of microbubbles on turbulent boundary layer skin friction. Ph.D. Thesis, The Pennsylvania State University.

- Madavan, N.K., Deutsch, S. & Merkle, C.L. 1984a Reduction of turbulent skin friction by microbubbles. Physics of Fluids 27, pp. 356-363.
- Madavan, N.K., Deutsch, S. & Merkle, C.L. 1984b The effects of porous material on microbubble skin friction reduction. AIAA Paper 84-0348, presented at 22nd AIAA Aerospace Sciences Mtg, Reno, Nevada.
- Madavan, N.K., Deutsch, S. & Merkle, C.L. 1985 Measurements of local skin friction in a microbubble-modified turbulent boundary layer. Journal of Fluid Mechanics 156, pp. 237-256.
- McCormick, M.E. & Bhattacharyya, R. 1973 Drag reduction of a submersible by electrolysis. Naval Engineers Journal 85, pp. 1-16.
- Mott Metallurgical Corporation 1988 Precision Porous Metals Engineering Guide, DB1000, Farmington Industrial Park, Farmington, Connecticut 06032.
- Pal, S., Merkle, C.L. & Deutsch, S. 1988 Bubble characteristics and trajectories in a microbubble boundary layer. Physics of Fluids 31, pp. 744-751.
- Schlichting, H. 1979 Boundary Layer Theory, McGraw-Hill Inc., New York.
- Schroeder, F.J. & Johnson, B. 1971 Design summary of the USNA 380 foot high performance towing tank. 16th American Towing Tank Conference.
- Souders, W.G. 1974 Turbulent boundary layer and viscous resistance of a submarine at high Reynolds number. Naval Ship Research and Development Center Report 4366.
- Tasaki, R., Yamasaki, T. & Muraoka, K. 1975 Increase of resistance due to air bubbles on the surface of a ship model. 14th ITTC Proceedings, Vol. 3, pp. 209-215.
- Thew, M.T., Lee, Y.T., Long, R.F. & Bragg, R. 1977 Experiments with soluble polymeric drag-reducing coatings. Second International Conference on Drag Reduction. Cambridge, England, Paper G2. BHRA Fluid Engineering.
- Thornton, W.A. 1974 Drag reduction of a hull by electrolysis. U.S. Naval Academy Trident Scholar Project Report No. 63.
- Walker, D.B. 1989 Viscous drag reduction for slender surface craft. U.S. Naval Academy Trident Scholar Project Report.
- Walsh, M.J. & Weinstein, L.M. 1978 Drag and heat transfer on surfaces with small longitudinal fins. AIAA Paper No. 78-1161, AIAA 11th Fluid and Plasma Dynamics Conference, Seattle, Washington.
- White, F.M. 1974 Viscous Fluid Flow. McGraw-Hill.